Journal of Nuclear Materials 133&134 (1985) 861–866

CORROSION OF FERROUS ALLOYS IN A FLOWING LITHIUM ENVIRONMENT

O.K. CHOPRA and D.L. SMITH

Materials Science and Technology Division, Argonne National Laboratory, Argonne, IL 60439, USA

Corrosion data on weight loss and internal penetration are presented for ferritic and austenitic stainless steels exposed for up to 6500 h at 700 and 755 K in a forced-circulation lithium loop. The results indicate that the dissolution rates for austenitic steels approach a steady-state value after an initial period (~ 1500 h) of much higher rates. The weight losses for ferritic steels follow a linear increase with time. The autenitic steels develop a porous ferrite layer after exposure to lithium. Measurements of the thickness of the ferrite layer follow the trends indicated by the weight loss data.

1. Introduction

Liquid lithium has long been considered an attractive blanket material for fusion reactors because of its acceptable tritium-breeding and efficient heat-transfer characteristics. The liquid lithium breeder/coolant concept is attractive because of the simplicity of the system. The major concerns arising from the use of lithium are corrosion/mass transfer, magnetohydrodynamic (MHD) effects, and degradation of mechanical properties of the containment material [1,2]. Uniform or selective dissolution, intergranular penetration, and interstitial element interactions can reduce the effective thickness of the wall. Deposition of the corrosion products may cause severe flow restrictions and excessive accumulation of radioactive material in unshielded regions. This paper presents information on the corrosion behavior of several ferrous alloys in a forced-circulation lithium loop in which the impurity content in lithium was controlled and monitored.

2. Experimental procedure

Corrosion tests were conducted in a test facility consisting of a forced-circulation lithium loop and an MTS closed-loop servohydraulic fatigue machine for performing mechanical tests in the liquid metal environment. A schematic diagram of the facility is shown in fig. 1. The liquid lithium system, which is constructed of Type 304 stainless steel, consists of a primary loop with three test vessels and a secondary cold-trap purification loop. Hot gettering was also used for controlling the interstitial elements in lithium. The quantity of lithium in the loop is ~ 20 l and lithium is recirculated at ~ 1 l/min in the primary loop. During the corrosion tests, the operating temperatures for the liquid lithium system were as follows: test vessel, 755 K; specimen-exposure vessel, 700 K; supply vessel, 673 K; primary pump oulet, 653 K; and cold trap, 488 K. Filtered lithium samples were obtained for analysis of nitrogen and carbon in lithium. The hydrogen concentration in lithium was determined by equilibrating yttrium samples in lithium and using the reported data on the distribution of hydrogen between lithium and yttrium [3].

During the initial period of operation (~ 6 months), the lithium system was shut down several times, owing to plugging of the flow meter and the pump section of the cold-trap loop. During these early phases of operation, the concentration of nitrogen in lithium increased to ~ 1200 wppm. The increase in nitrogen was attributed to contamination from the mechanical test fixture and inadequate impurity control. On each occasion the plugged section was replaced with a new pipe. Lithium from the plugged regions of the loop was dissolved in a solution of methyl alcohol and water, and the residue was analyzed by energy dispersive X-ray (EDAX) and X-ray diffraction analyses. A strong odor of ammonia was detected during the dissolution of lithium and the solution turned dark yellow or green. Scanning electron micrograph and EDAX analyses of the metallic residue collected after the first shutdown are shown in fig. 2. The residue consisted of large faceted crystals and small globular particles composed of nickel and manganese. These particles were identified by X-ray diffraction as the tetragonal MnNi and cubic $MnNi_3$ phases, which are paramagnetic below 633 K (360°C). Residues collected from subsequent shutdowns contained large particles of pure iron or iron–nickel compounds. Chromium was not detected in the metallic residue.

The results indicate that plugging was caused by accumulation of magnetic crystals under the pump coil or flow meter magnet. The increase in nitrogen concentration in the lithium resulted in excessive dissolution and mass transfer of various constituents of the stainless steel vessel. Chromium was present in the lithium, probably as chromium nitride, which dissociated into ammonia and lithium–chromium oxide when the lithium was dissolved in methyl alcohol and water.

The nitrogen level in the lithium loop was reduced to < 100 wppm by hot trapping with Ti and Zr and by means of dissolved getters, such as calcium. A magnetic trap was installed upstream from the flow meter and pump sections of the cold-trap loop. Corrosion data were obtained from flat specimens, ~ 70 × 10 × 0.3 mm

0022-3115/85/$03.30

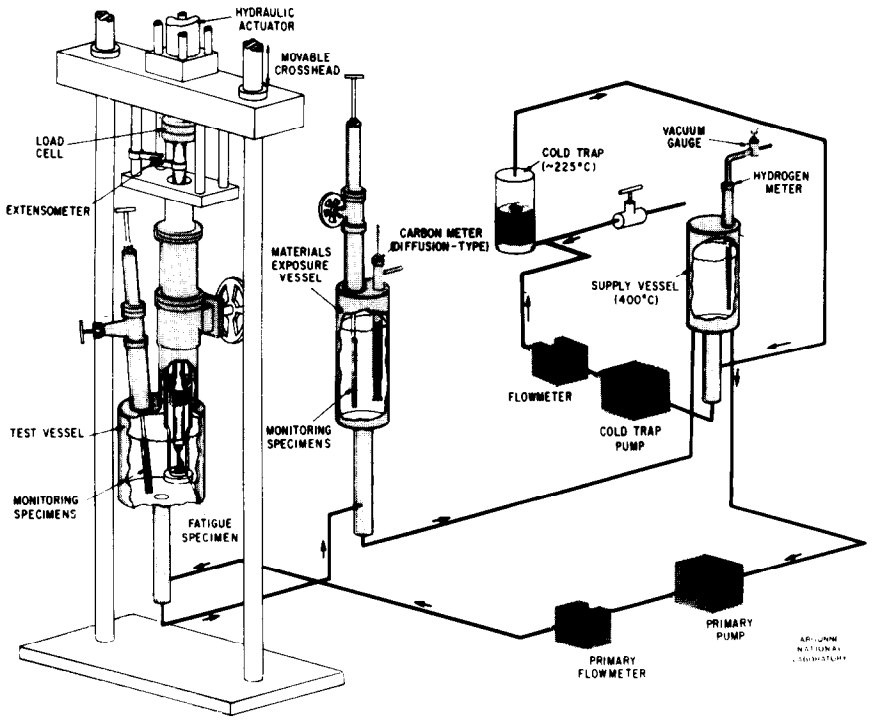

Fig. 1. Schematic of facility for fatigue testing in lithium.

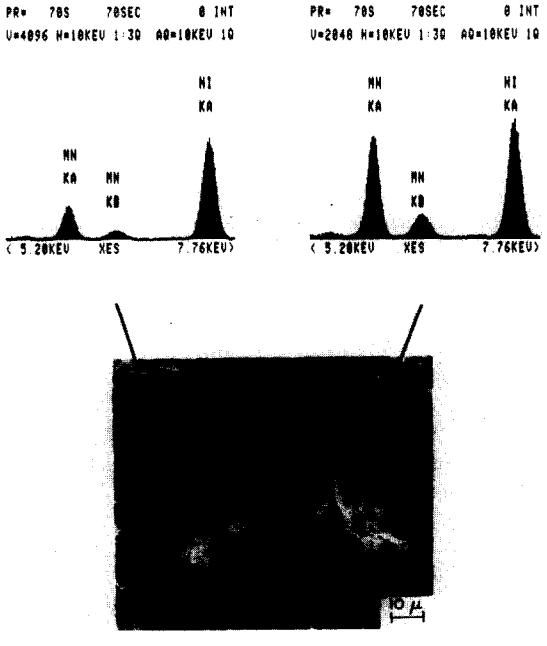

Fig. 2. Micrograph and EDAX analyses of the metallic residue collected from the pump coil section of the plugged cold-trap pipe removed after the first shutdown.

in size, of Type 316 stainless steel (SS), prime candidate alloy (PCA), Fe–9Cr–1Mo steel, and HT-9 alloy exposed to flowing lithium at 755 and 700 K (482 and 427°C) for up to 6500 h. Tests at 755 K were conducted in the test vessel simultaneously with the 700 K tests in the material exposure vessel. Similar test fixtures were used for the two vessels. During the corrosion tests, the concentrations of carbon and hydrogen in lithium were ~ 10 and 120 wppm, respectively, and the nitrogen content was maintained between 50 and 100 wppm. The compositions of various alloys are given in table 1. The ferritic steels were exposed in the normalized and tempered condition. Two different heat treatments were employed for the autenitic steels. For Type 316 SS the treatments were solution anneal (SA) and SA plus 20% cold work (CW). For PCA the treatments were SA plus 25% CW (treatment A3) and SA plus 8 h at 1073 K plus 25% CW plus 2 h at 1023 K (treatment B2). The specimens were periodicially removed from the loop for weight change measurements. Specimens exposed to lithium were examined metallographically for measurements of the depth of internal corrosive penetration. Energy dispersive X-ray analysis were performed to determine the distribution of major elements in the specimens. The depth of internal penetration was determined from the difference between the initial thickness of the specimen and the sound metal remaining (i.e., unreacted metal) after exposure to lithium.

Table 1
Chemical composition of austenitic and ferritic steels

Alloy	Content (wt%)									
	Cr	Ni	Mo	Mn	Si	P	S	C	N	Other
PCA	14.0	16.2	2.3	1.8	0.40	0.010	0.003	0.05	0.010	0.24Ti
316 SS	17.0	13.4	2.49	1.9	0.64	0.024	0.020	0.07	0.034	
HT-9	12.0	0.6	1.03	0.5	0.22	0.006	0.002	0.21	0.003	0.32V, 0.5W
9Cr–1Mo	8.8	–	0.92	0.4	0.36	–	–	0.098	0.011	0.21V, 0.06Nb

3. Results and discussion

3.1. Ferritic steels

The weight losses of the various specimens exposed to flowing lithium at 755 and 700 K were obtained as a function of time. At both temperatures, the weight loss of HT-9 and Fe–9Cr–1Mo steel increased linearly with exposure time. The results at 700 K are shown in fig. 3. Each symbol type in the figure represents weight loss for a single specimen after various exposure times. After exposure to lithium, all specimens exhibited a dimpled or pebbled appearance (fig. 4). The dimpled structure developed during the initial ~ 500 h exposure and did not change significantly with longer exposure times. Fig. 3 shows a 0.5 to 0.8 g/m^2 loss in weight for all the specimens after the initial exposure to lithium. This weight loss may be attributed to the formation of the dimpled structure.

The corrosion data indicate significant differences in weight loss for specimens that were exposed during different test runs. For example, the weight losses for specimens shown by triangle and diamond symbols in fig. 3 are 30 to 50% lower than for the other specimens. However, duplicate specimens exposed at the same time always showed comparable values of weight loss. A similar behavior was also observed for the autenitic Type 316 SS and PCA specimens. Such differences in weight loss cannot be attributed to experimental scatter alone; small variations in the impurity content in lithium, particularly the concentration of nitrogen in lithium, can also influence the dissolution behavior. For example, a set of ferritic and autenitic steel specimens exposed for 2000 h at 755 K in lithium containing 200 wppm nitrogen showed a factor of 2 to 4 greater weight loss than specimens exposed in lithium containing < 100 wppm nitrogen. Recent studies indicate that nitrogen can react with alloy elements and lithium to form stable ternary nitrides, such as Li_9CrN_5 and Li_3FeN_2, and thus accelerate the dissolution process of ferrous alloys [4].

The weight losses for ferritic steels can be expressed by a linear relationship with time, given by

$$W = A + Rt, \tag{1}$$

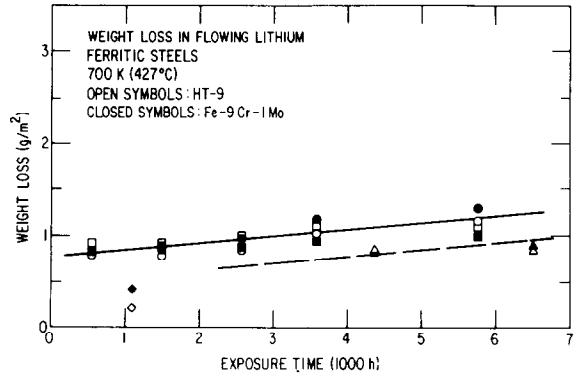

Fig. 3. Weight loss versus exposure time for ferritic HT-9 and Fe–9Cr–1Mo steel exposed to flowing lithium at 700 K. Each symbol type represents weight loss for a single specimen after various exposure times.

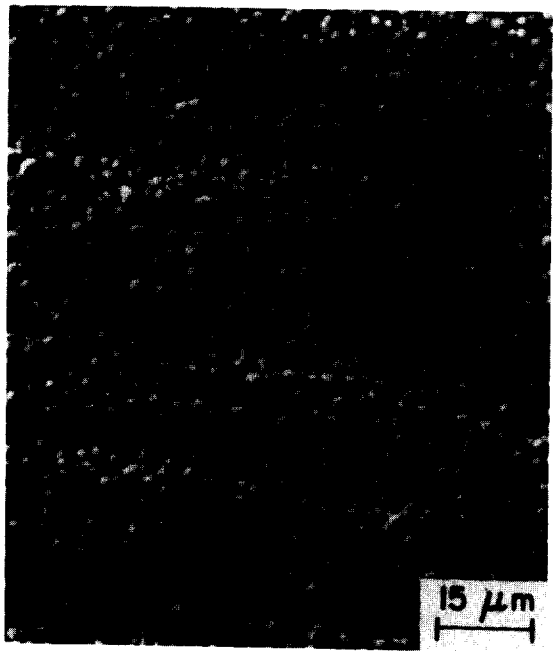

Fig. 4. Micrograph of the surface of HT-9 alloy exposed to lithium at 755 K.

where weight loss is in g/m^2, R is the dissolution rate, A is the intercept, and time t is in hours. The average dissolution rates for both HT-9 and Fe–9Cr–1Mo steels are 0.16 and 0.07 mg/m^2 h at 755 and 700 K, respectively. The dissolution rate decreases with a decrease in temperature. These values of dissolution rates obtained at 755 and 700 K in a cold-trapped forced-circulation lithium loop are consistent with the rate of 0.4 mg/m^2 h observed for HT-9 alloy in a lithium thermal convection loop (TCL) at 733 K [5]. The nitrogen concentration in lithium in the latter test was reported to be < 100 wppm.

Metallographic examination of the cross section of the lithium-exposed specimens indicated no internal corrosion. EDAX analyses revealed slight depletion of chromium to a depth of ~ 10 μm from the surfaces of the various specimens.

3.2. Austenitic steels

The austenitic steel specimens also developed a dimpled or pebbled appearance after exposure to lithium. Weight loss data for Type 316 SS and PCA indicate that the dissolution rates reach a steady-state value after an initial 1500 h period of rapidly decreasing rates. The results for Type 316 SS and PCA exposed to lithium at 700 K are shown in fig. 5. The weight losses for austenitic steels are more than an order of magnitude greater than those for the ferritic steels. For the various austenitic steels, the loss in weight increases in the following order: annealed Type 316 SS, 20% CW Type 316, and PCA. As observed for the ferritic steels, the austenitic steel specimens which were exposed during different test runs show differences in weight loss, whereas duplicate specimens exposed at the same time show similar weight loss. However, for each alloy, the steady-state data from different test runs yield comparable dissolution rates.

After exposure to lithium, the austenitic stainless steels developed a porous ferrite layer that was significantly depleted in nickel. The distribution of major elements across the ferrite layers on PCA and Type 316 SS exposed to lithium at 700 K is shown in fig. 6. Both steels show an ~ 10 μm thick surface region depleted in chromium and the entire ferrite layer is significantly depleted of nickel. The concentration of nickel decreases abruptly across the ferrite-austenite boundary. A typical EDAX analysis of the surface of Type 316 SS yields ~ 1% nickel and ~ 10% chromium.

Measurements of internal penetration indicate that the thickness of the ferrite layer formed on annealed or 20% CW Type 316 SS in lithium at 755 K is comparable to that at 700 K. For a given time, the thickness of the ferrite layer on PCA was greater than on Type 316 SS. Internal penetration for Type 316 SS exposed to lithium at 755 and 700 K is plotted as a function of time in fig. 7. Most of the data can be represented by a power-law relationship with a value of 0.34 for the time exponent.

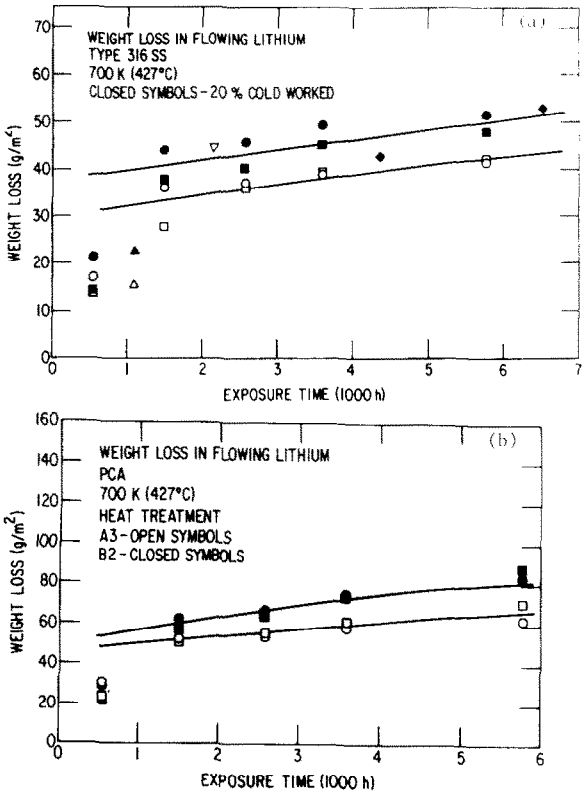

Fig. 5. Weight loss versus exposure time for (a) Type 316 SS and (b) PCA exposed to flowing lithium at 700 K. Each symbol type represents weight loss for a single specimen after various exposure times.

Such a relationship yields a growth rate of 22 μm/y at 5000 h.

The steady-state dissolution rates were obtained from eq. (1) by using weight loss data for exposure times of > 1500 h and are shown as solid lines in fig. 5. The average dissolution rates for annealed or 20% CW Type 316 SS were 1.6 and 2.1 mg/m^2 at 755 and 700 K, respectively. The corresponding dissolution rates for PCA were a factor of 2 to 4 greater than for Type 316 SS, i.e., the rates at 755 and 700 K were, respectively, 3.3 and 3.7 mg/m^2 h for PCA (A3) and 5.8 and 6.4 mg/m^2 h for PCA (B2). The results indicate that for the various austenitic steels, the dissolution rates at 700 K are slightly higher than at 755 K. The data at 700 and 755 K were obtained in two separate vessels of the lithium loop, in which the lithium flow was from the high- to the low-temperature vessel. The differences in loop geometry or downstream effects may be responsible for the anomalous results. However, different corrosion mechanisms may dominate the dissolution behavior in different temperature regimes. For example, corrosion data in lithium TCLs indicate that the depletion of chromium from Type 316 SS increases with an in-

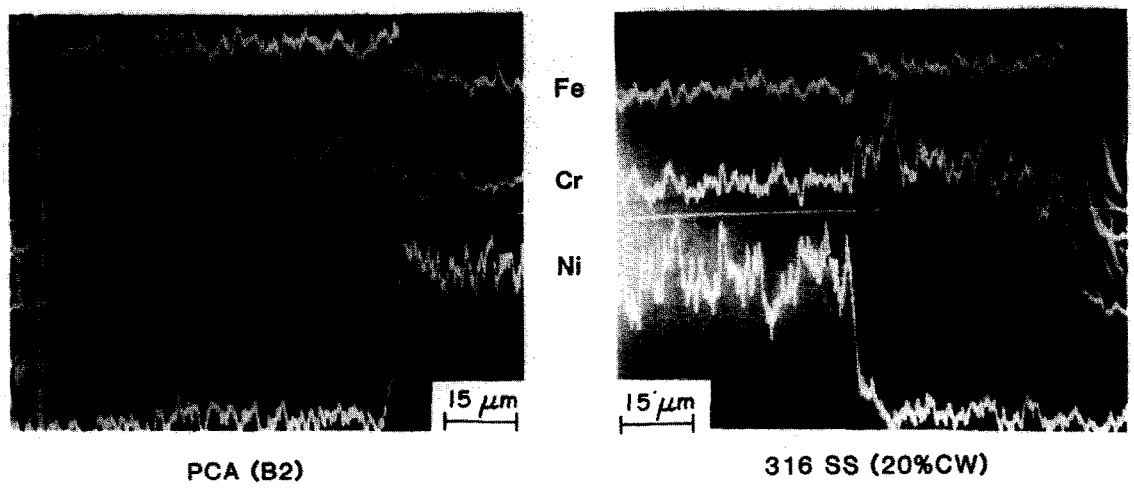

Fig. 6. Micrographs and concentration profiles for major elements across the ferrite scale of PCA and Type 316 SS exposed to lithium at 700 K.

crease in temperature; the average chromium concentrations of the surface of Type 316 SS decreased from ~ 7% at 813 to ~ 3% at 873 K [6]. The present data yield chromium concentrations of ~ 10% for Type 316 SS exposed to lithium at 700 or 755 K. Corrosion/mass transfer data in lithium TCLs operated at a maximum temperature of 873 K and a minimum temperature of 723 K showed chromium-rich deposites followed by iron-rich deposits in the cold leg of the loop [7]. For the present study, nickel-rich crystals were observed in the cold-trap secondary loop maintained at 498 K. Such differences in mass transfer behavior arise from differences in maximum temperature, ΔT, geometry, etc.

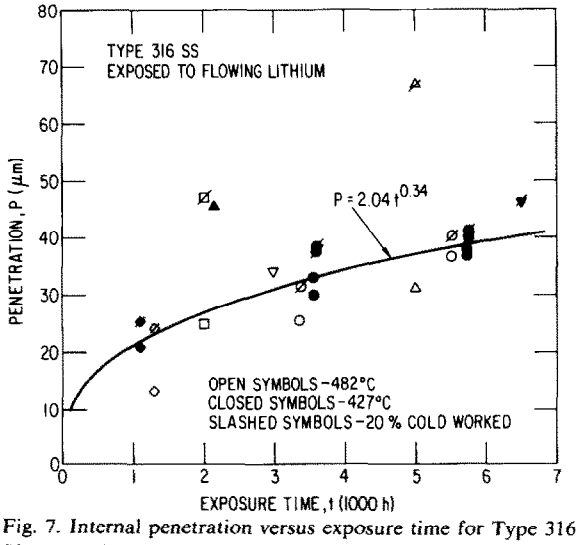

Fig. 7. Internal penetration versus exposure time for Type 316 SS exposed to lithium of 700 and 755 K. Each symbol type represents penetration for a single specimen after various exposure times.

of the liquid lithium system. Additional data over a wide range of loop temperature and system parameters are required to establish the influence of these parameters on the dissolution behavior of austenitic steels in lithium.

For the austenitic steels, the initial stage of high dissolution rates corresponds to the formation of a ferrite layer which results from preferential leaching of nickel, and to a lesser extent, chromium from the surface of the steel. A similar behavior is observed for austenitic stainless steels exposed to flowing sodium environment. A steady-state dissolution rate is attained in sodium when the elements being dissolved from the ferrite layer are in proportion to their concentration in the steel. Consequently, at steady state, the movement of the ferrite–austenite boundary is the same as the recession of the dissolving surface, such that the thickness of the ferrite layer is constant [8]. Measurements of the thickness of the ferrite layer indicate that such a "stoichiometric" steady-state dissolution behavior may not be achieved in a flowing lithium environment. Data for internal penetration of Type 316 SS yield a growth rate of ~ 22 μm/y whereas the weight loss measurements give an average dissolution rate of ~ 1.9 mg/m^2 h, which corresponds to a uniform recession of only ~ 2 μm/y.

4. Summary

The corrosion data in flowing lithium at 755 and 700 K indicate that the weight losses of ferritic HT-9 and Fe–9Cr–1Mo steel follow a linear law with time and yield constant dissolution rates of 0.16 and 0.07 mg/m^2 h at 755 and 700 K, respectively. The weight losses for the austenitic Type 316 SS and PCA are more than an

order of magnitude greater than for ferritic steels. The dissolution rates for austenitic steels decrease significantly during the initial exposure period and reach a steady-state value after ~ 1500 h. The dissolution rates for PCA are a factor of 2 to 4 greater than for Type 316 SS. The steady-state dissolution rates for both austenitic steels at 755 and 700 K are anomalous, with slightly higher rates at 700 K than at 755 K. Different corrosion mechanisms may dominate the dissolution behavior in different temperature regimes. Additional data over a wide range of system parameters (lithium purity, temperature, ΔT, loop geometry, etc.) are required to establish the influence of these parameters on the dissolution rates of austenitic steels. The austenitic stainless steels develop a porous ferrite layer after exposure to lithium. Measurements of the thickness of the ferrite layer indicate that a "stoichiometric" steady-state dissolution behavior normally observed for austenitic steels in a sodium environment may not be achieved in a flowing lithium environment.

Acknowledgement

Work was supported by the Office of Fusion Energy, US Department of Energy.

References

[1] O.K. Chopra and P.F. Tortorelli, J. Nucl. Mater. 122–123 (1984) 1201.
[2] P.F. Tortorelli and O.K. Chopra, J. Nucl. Mater. 103–104 (1981) 621.
[3] D.L. Smith, R.H. Lee and R.M. Yonco, in: Proc. Second Int. Conf. on Liquid Metal Technology in Energy Production, US Department of Energy Report CONF-800401-P1 (1980) p. 272.
[4] M.G. Barker, P. Hubberstey, A.T. Dadd and S.A. Frankham, J. Nucl. Mater. 114 (1983) 143.
[5] P.F. Tortorelli and J.H. DeVan, Proc. Topical Conf. on Ferritic Alloys for Use in Energy Technologies (AIME, 1983) in press.
[6] P.F. Tortorelli and J.H. DeVan, Microstructural Science (1983) in press.
[7] P.F. Tortorelli and J.H. DeVan, Proc. Third Int. Conf. on Liquid Metal Engineering and Technology in Energy Production, Oxford, England (1984) in press.
[8] E.G. Brush, General Electric, GEAP-4832 (1965).